Precipitation leads the long-term vegetation increase in the conterminous United States drylands

Yuhe Chang[1,*], Alexander J. Winkler[2], Amirhossein Noori[1], Yuri Knyazikhin[1], and Ranga B. Myneni[1]

[1]Department of Earth and Environment, Boston University, Boston MA 02155, USA
[2]Max-Planck-Institute for Biogeochemistry, 07745 Jena, Germany
[*]Author to whom any correspondence should be addressed
Email: yhchang@bu.edu

Abstract

Drylands, encompassing over 40% of the conterminous United States (CONUS), are crucial to the global carbon cycle and highly susceptible to climate change. However, Earth system models offer conflicting projections of future drought and vegetation activity in North America, and in-depth analyses of the long-term changes in greenness and its relationship with underlying climate drivers, considering both spatial and temporal variations at the ecosystem scale, are lacking. This study analyzes 20-year (2001-2020) MODIS NDVI observations to assess greening trends in CONUS drylands and their relationship with climate drivers at 1km spatial resolution. Results indicate a large scale and systematic greening trend, particularly in the northern Great Plains (NGP) region. Using an empirical linear attribution approach and Empirical Orthogonal Function (EOF) analysis, we uncover varied relationships between greenness trends and climate drivers, particularly highlighting the dominant role of increased precipitation in driving the observed greening. Trend analysis reveals that while rain use efficiency (RUE) remains stable in most areas, increases in the NGP region suggest potential CO2 fertilization effects (CFE), while decreases in southern states correlate with rising temperatures. We also develop an efficiency-based model featuring RUE which successfully reproduces historical NDVI, re-confirming the dominant influence of precipitation in local greenness interannual variability. However, CMIP6 projections for 2021-2040 under the "Regional Rivalry" scenario (SSP370) paint a worrying picture, with projected browning in the NGP region and states near the 42°N latitude, contrasting recent greening trends. This potential reversal underscores the vulnerability of these ecosystems to future climate change, highlighting the need to consider both historical trends and future climate projections when assessing the resilience of drylands ecosystems. Overall, our work re-emphasizes the significance of water availability to drylands vegetation growth and contributes to a more comprehensive understanding of carbon-water cycling in arid and semi-arid regions.

Introduction

Dryland ecosystems play a critical role in the global carbon cycle, strongly contributing to the trend and inter-annual variability of the global terrestrial carbon sink, due to their high sensitivity to inter-annual climate variability (Ahlström et al., 2015). Drylands feature a scarcity of water and are particularly susceptible to climate change (Lian et al., 2021), especially variations in precipitation and temperature. Recent studies indicate declining future of water availability in drylands as climate projections show that drylands will experience increased warming, drought frequency, and evaporative demand at rates faster than the global average (Lehner et al., 2017; Bradford et al., 2020; Feng & Fu, 2013; Müller & Bahn, 2022). Drylands tend to be more severely impacted by drought events which stress local vegetation and subsequently affect their carbon sequestration capabilities. Conversely, as droughts exacerbate due to global warming, the increasing level of CO_2 concentration is reported to benefit photosynthesis through the CO_2 fertilization effect (CFE) (Gonsamo et al., 2021), as vegetation can keep their stomata closed for longer durations to conserve water for photosynthesis while maintaining a consistent level of intercellular CO_2 concentration (Zhang et al., 2022).

Discrepancies between global and regional scale studies regarding the present trajectories of drylands are evident. Several analyses have indicated a global increase in aridity within drylands, resulting in significant and sudden alterations in numerous ecosystem characteristics (Berdugo et al., 2020). A considerable portion of drylands has been reported to experience desertification and soil deterioration due to unsustainable land management practices exacerbated by human-induced climate variations (Burrell et al., 2020). However, these assertions have been challenged with claims that conventional aridity metrics inadequately represent the land-based water cycle, thereby producing questionable outcomes from Dynamic Global Vegetation Models (DGVMs) (Berg & McColl, 2021). In contrast, trends of greening and increased vegetation activity across diverse dryland environments have been reported in regional studies (Hänke et al., 2016; He et al., 2019; Li et al., 2022). Various factors contribute to this discrepancy in findings, with differing spatial resolutions of input datasets emerging as a pivotal factor. Coarse-resolution pixels consist of mixed land surface signals, leading to ambiguity in temporal trend analyses when compared with outcomes derived from datasets at finer resolution (Ji & Brown, 2022; Zhang et al., 2023). Spatial grain needs to be explicitly considered in dryland ecosystem which is constrained by precipitation when examining the influence of climate variables on local vegetation dynamics as experiments have shown that the effects of precipitation manipulation on plants are strongest at the smallest spatial scale compared to other environmental factors (Korell et al., 2021).

Drylands in the conterminous United States (CONUS) account for more than 40 % of the territory, encompassing a diverse array of arid and semi-arid ecosystems. These regions, including parts of the Great Basin, the Colorado Plateau, the Sonoran and Mojave Deserts, and most of the Great Plains, exhibit pronounced climatic variability. This climatic regime leads to a persistent water deficit, exerting a significant influence on soil moisture availability and vegetation dynamics. The temperature profiles in these regions are marked by extreme seasonal and diurnal variations. The high variability in temperature and precipitation, both spatially and temporally, underpins the ecological processes and biotic adaptations in these arid landscapes.

Few research endeavors have been focused on exploring the prolonged alteration in vegetation over an extensive time-frame in conjunction with contemporary climate fluctuations within CONUS on a continental scale, among global and site-specific investigations. This research addresses this gap by examining greenness trends in the natural CONUS drylands from 2001 to 2020, utilizing long-term satellite-derived Normalized Difference Vegetation Index (NDVI) data from MODIS. This study delves into the primary climatic drivers at 1km spatial resolution through regression-based attribution and empirical orthogonal function (EOF) analysis, assessing associations from both temporal and spatial perspectives. To evaluate the local ecosystem's functionality, adaptability, and reaction to climatic changes, the study specifically scrutinizes the long-term trends of rain use efficiency (RUE) across the entire research area. Furthermore, we develop a simplified model based on RUE to replicate observed NDVI trends and annual variations, projecting NDVI alterations in CONUS drylands for the subsequent two decades (2021-2040) utilizing downscaled CMIP6 precipitation projections.

Data and methods

Terra MODIS Vegetation Index Products

The NDVI observations in this study comes from Terra MODIS Vegetation Index Products Collection 6.1 (MOD13Q1 v061) (Didan, 2021, DOI:10.5067/MODIS/MOD13Q1.061) which provides consistent, spatial, and temporal comparisons of global terrestrial vegetation conditions. Normalized difference vegetation index (NDVI) is provided as 16-day composite layers at 250-meter spatial resolution. To maintain the consistency of the data sources across all years, only Terra MODIS products are used to acquire NDVI observations for its longer record compared to Aqua products. Only data for 2001 to 2020 is used. In addition, to exclude the effects of cloud cover, surface reflectance inconsistences, and other potential artifacts, we mask out pixels related to bad quality according to the built-in VI Quality band. We also adopt a upward-smoothing approach to fill the data gap (Chen et al. 2004).

MODIS Land Cover Type Products

The land cover (LC) type information is obtained from MODIS Terra and Aqua combined Land Cover Type products Collection 6.1 (MCD12Q1 v061) (Friedl & Sulla-Menashe, 2022, DOI:10.5067/MODIS/MCD12Q1.061) which provide global land cover types at yearly intervals from 2001 to 2022. The spatial resolution of MCD12Q1 is 500-meter. This study specifically uses the International Geosphere-Biosphere Programme (IGBP) classification scheme. To focus on vegetation change in natural drylands and avoid influence of human intervention, pixels classified as one of following four land cover types, Croplands, Urban and Built-up Lands, Cropland/Natural Vegetation Mosaics (Semi-Croplands), and Water Bodies, in any LC layers within the two-decade study period are further masked out. To maintain spatial gridding consistency across datasets, the final decision is made on a resampled 1km reference LC composite map.

Meteorological data

Data of precipitation, daily maximum temperature, and incoming shortwave radiation flux density used in this study are collected from Daymet: Daily Surface Weather Data (Version 4) (Thornton et al., 2022, available at https://doi.org/10.3334/ORNLDAAC/2129). This dataset offers persistent and continuous gridded estimations of daily weather and climatological variables at 1km spatial resolution and over an extended period (1980~2022), which is arguably the most accurate and updated meteorological dataset currently available for CONUS. These estimations are derived by interpolation and extrapolation of ground-based observations through statistical modeling techniques (Thornton et al., 2021).

Study Region

This study focuses on CONUS drylands, defined as areas receiving less than 600 mm of annual total precipitation (ATP). Figure 1 illustrates the spatial patterns of key climate variables across the study region, highlighting distinct regional differences. Precipitation tends to be the primary limiting factor for vegetation growth in CONUS drylands, particularly in the south (Nemani et al. 2003). While temperature exerts a secondary influence, its importance increases with latitude. This is reflected in the three distinct climate zones evident in Figure 1A: the Northern Great Plains (NGP) region, encompassing Montana, Wyoming, North Dakota, South Dakota, and Nebraska, is characterized by a relatively wet and cool environment and is the focus of further investigation in this study; the Southern Great Plains have a wet and hot climate; and the Southwestern states are dominated by dry and hot conditions. Figure 1B further reveals the spatial distribution of incoming shortwave radiation, which exhibits variation primarily along latitudinal gradients.

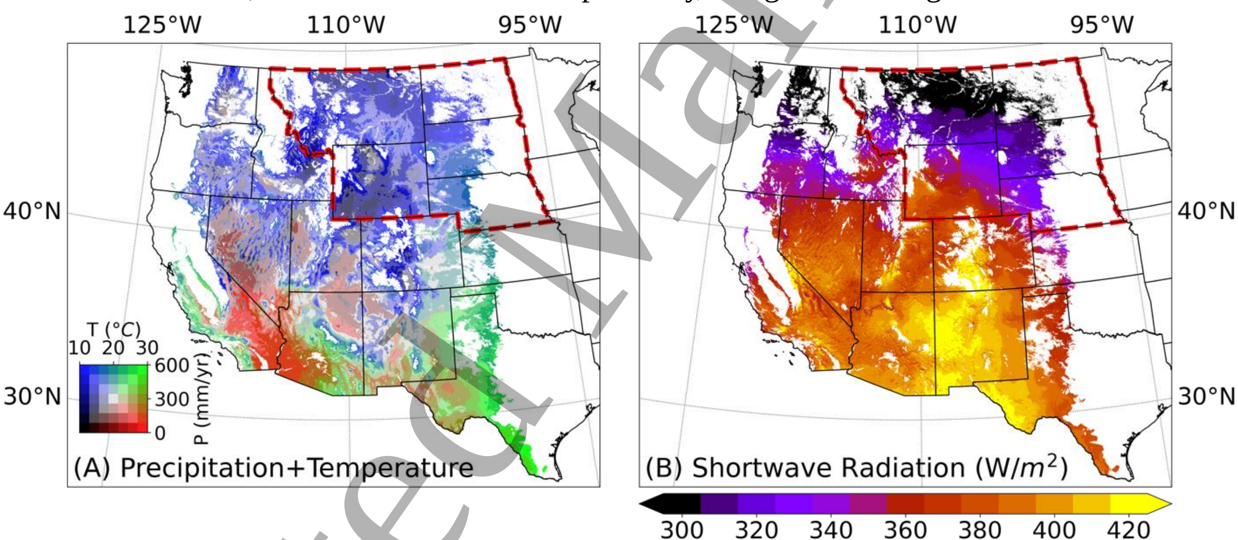

Figure 1. Climatology (2001~2020) spatial distribution of climate drivers in CONUS drylands (ATP < 600mm/year). The enclosed area defines the zoom-in study region in the northern Great Plains. (A) Joint spatial distribution of annual total precipitation and annual mean daily maximum temperature. Distinct regional patterns can be observed; (B) Spatial distribution of daytime incident shortwave radiation flux density. Its value varies mainly along latitude.

Temporally Summarized Datasets

The primary challenge of analyzing the impacts of interdependent and correlated climatic factors on the trend of greenness is to identify climate indices that effectively capture the "period of climatic influence" (Ahlström et al., 2015). Because of that, two types of datasets, annual and growing season summarized datasets, are created for NDVI and three climatic variables from original monthly datasets. Annual summarized data has the merit of being simple and is more useful for studying extensive areas where heterogeneity in growing seasons is present. Growing season summarized data is in general a better proxy for quantifying the direct influence of climatic variables on vegetation growth. By adopting growing season identifying methods introduced in Körner et al., 2023, a period of six months (April~September) is determined as the growing season (monthly resolution) for the NGP region (Figure S1). Corresponding growing season average/sum datasets are created for all variables.

Trend Analysis

In this study, trends are evaluated using the Mann-Kendall (MK) test, a non-parametric method well-suited for detecting trends in vegetation indices without assuming data normality (de Jong et al., 2011; Fensholt et al., 2012; Chen et al., 2019). Specifically, we employ the modified pre-whitening MK test (Yue et al., 2002), which reduces potential false positives by mitigating autocorrelation in time series data. For computational efficiency, the pyMannKendall package (Hussain & Mahmud, 2019) source code is adapted for compatibility with C++. A significance level (α) of 0.1 is set, indicating that a time series with $p \leq 0.1$ exhibits a statistically significant trend.

Empirical Linear Attribution Method

A multiple linear regression (MLR) model is employed to attribute observed greenness changes to the dominant climate drivers. MLR has been in studying spatial-temporal variation of LAI (Zhang et al., 2024), soil properties (Forkuor et al., 2017), and droughts (Kim et al., 2020). Similar methods are used to assess contributions of anthropogenic and natural factors to global climate change (Canty et al., 2013; Lean & Rind, 2008; Stern & Kaufmann, 2014). The regression coefficients in MLR provide conceptually simple and direct insights into the strength and direction of the relationship between NDVI and each climate variable, which makes it easy to assess the relative contributions of different drivers. This approach assumes predictor independence. To ensure this, the correlation matrix is evaluated prior to analysis. The model takes the following form:

$$\Delta V = \alpha + \beta_1 \Delta P + \beta_2 \Delta T + \beta_1 \Delta R_{sw} + \epsilon \quad (1)$$

where the Δ terms are normalized anomalies of each variable, β_i is the associated coefficient, α is the intercept, and ϵ is the error term, and V, P, T and R_{sw} denote greenness (NDVI in this study), precipitation, temperature, and shortwave radiation, respectively.

Anomalies are calculated as deviations from climatological means, and normalization is achieved by dividing by the Euclidean (L2) norm. This allows each time series to be viewed as a unit vector in multidimensional space. By evaluating the coefficients, the interannual variability of NDVI in the study region can be attributed to its potential climate drivers.

Empirical Orthogonal Function (EOF) Analysis

EOF analysis is commonly used to reduce the dimensionalities of the datasets and extract the leading modes of variability which are often assumed to relate to various physical processes (Volkov et al., 2022). It has vast applications in environmental studies to analyze spatiotemporal patterns of climate variables (Roundy, 2015; Tippett & L'Heureux, 2020; Werb & Rudnick, 2023;

Zhang et al., 1997). We employ EOF analysis in this study to assess the intercorrelation between NDVI and selected climate variables in both spatial and temporal domains. For each mode of a climate variable, a spatial regression map (EOF_i) and the corresponding principal component (PC_i) are generated, and they are then compared with the EOF analysis results of NDVI using different techniques. A python package (eofs) (Dawson, 2016) is used for performing the analysis.

Rain use efficiency and efficiency-based model

Rain Use Efficiency (RUE) refers to the ratio of Aboveground Net Primary Production (ANPP) to total precipitation, and it is an effective index for assessing ecosystem productivity of drylands (Le Houérou, 1984). The linear relationship between ANPP and NDVI has been well studied and established (Myneni & Williams, 1994; Holm et al., 2003; PRINCE, 2007; Rasmussen, 2010; Wessels et al., 2006; Xue et al., 2017). Temporal integrated NDVI ($\sum$NDVI or iNDVI) is found to be a consistent proxy for ANPP (Chang et al., 2018; Dardel et al., 2014; Fensholt et al., 2013; Kaptué et al., 2015; Paruelo et al., 1999). In this study, the temporal average NDVI ($\overline{\mathrm{NDVI}}$), which is conceptually equivalent to iNDVI (only differ by a constant factor), is used for RUE calculation,

$$\mathrm{RUE} = \frac{\overline{\mathrm{NDVI}}_n}{\sum_1^n P_i} \quad (2)$$

where n represents the number of months, which varies depending on the period (annual or seasonal) for which the RUE is evaluated, and i denotes the month.

To rule out the climate influence on vegetation beyond the target period, which is often defined as the "zero intercept" difficulty when using NDVI instead of ANPP for RUE calculation (Dardel et al., 2014; Verón et al., 2005). A concept of baseline average NDVI ($\overline{\mathrm{NDVI}}_b$) is proposed in this study. It is assumed to be proportionate to a portion of in-situ ANPP which is not attributable to the precipitation descended within the target period but rather to the stored soil moisture or underground water. $\overline{\mathrm{NDVI}}_b$ in this study is taken as the minimum monthly mean NDVI during a year for annual case, and the monthly mean NDVI over three non-growing season months prior to the growing season for seasonal case. The improved RUE calculation is then expressed as below,

$$\mathrm{RUE} = \frac{\overline{\mathrm{NDVI}}_n - \overline{\mathrm{NDVI}}_b}{\sum_1^n P_i} \quad (3)$$

The regional average RUE is calculated as the ratio of pixel-wise sum of NDVI to the pixel-wise sum of total precipitation,

$$\overline{\mathrm{RUE}} = \frac{\sum_1^N \left(\overline{\mathrm{NDVI}}_{n,p} - \overline{\mathrm{NDVI}}_{b,p}\right)}{\sum_1^N \sum_1^n P_{i,p}}, \quad (4)$$

where N denotes the pixel count of the target region, and p denotes the pixel index.

Based on RUE, we proposed a efficiency-based model to reproduce the historical NDVI interannual variability and project future conditions of CONUS drylands vegetation. This model is adapted from an open-loop linearized model, first introduced in Wang et al., 2006, which is established for semi-arid grassland regions in the North America to quantify the vegetation dynamics and contribution of precipitation to local vegetation growth. With the main difference that we aim to study vegetation change and its correlation with precipitation seasonally and annually instead of monthly in its original work, we can safely regard that NDVI can be informed by contemporary precipitation, given the prolonged study period and transit nature of precipitation in drylands environments. The modified model has the following form,

$$V_t = \alpha V_{b,t} + \beta P_t + \epsilon_t \quad (6)$$

where V_t and $V_{b,t}$ denote the temporal average NDVI and corresponding baseline NDVI, α and β denote the persistence rate of greenness and RUE, respectively, P_t is the total precipitation of interested period.

To account for the widely observed negative correlation between RUE and precipitation (RUE decreases as precipitation increases) (Huxman et al., 2004; Zhang et al., 2020), RUE (β) in this model is calculated as the sum of its climatology value and response to precipitation anomaly (ΔP) by coefficient k, which has the following form,

$$\beta = \beta_0 \cdot (1 + k\Delta P_t) \quad (7)$$

When $V_{b,t}$ is taken as its climatology value, the only independent variable in this model is annual or seasonal total precipitation.

Future Projections from downscaled CMIP6 simulations

The proposed efficiency-based model is in addition used for projecting the future greenness conditions of CONUS drylands, with the state-of-the-art CMIP6 climate projections as inputs (Eyring et al., 2016). WorldClim (worldclim.org) provides the latest downscaled CMIP6 projections at 30 arc seconds, processed and calibrated with WorldClim v2.1 (Fick & Hijmans, 2017) as baseline climate. 20-year climatology monthly precipitation predictions for the future (2021~2040) are obtained from six global climate models (GCMs), which are GFDL-ESM4 MIROC6, MPI-ESM1-2-HR, EC_Earth3-Veg, UKESM1-0-LL, and CMCC-ESM2 for the boundary conditions given by the SSP370 scenario (O'Neill et al., 2016). SSP370 is specifically selected because the projection period in this study (2021-2040) is not far into the future. Because of that, we predict the trajectory of our study region, assuming that there is no major change in the environment policies for the next two decades. SSP370 is the one closest to the "business as usual" scenario among all available SSPs.

Results and discussions

Inter-annual NDVI trend and relationship with climate drivers

The 20-year trend analysis of annual mean NDVI in CONUS drylands (Figure 2A) reveals a predominance of non-significant trends, with the notable exception of the Northern Great Plains (NGP) region, which exhibits extensive and clustered greening. In other states, significant greening trends are fragmented and sparsely distributed. Arizona also demonstrates notable greening trends, though less pronounced than in the NGP and weaker in magnitude. Browning trends are minimal across the study area, occurring primarily at a micro-scale, with slightly higher prevalence in New Mexico and west Texas. Focusing on the NGP region, Figure 2B illustrates the growing season mean NDVI trend, revealing a larger proportion of pixels with increasing trends compared to the annual mean NDVI analysis. Figure 2C compares the time series of annual mean NDVI for all CONUS drylands with the seasonal mean NDVI of greening pixels in the NGP. As confirmed by the MK test, the annual mean NDVI of all dryland pixels shows no significant trend over the study period due to the relatively small proportion of greening pixels. In contrast, within the NGP region, the seasonal mean NDVI of greening pixels exhibits a consistent and steady increasing trend despite clear interannual variability. Figure S2 shows the LC map for CONUS drylands. Grasslands dominate CONUS drylands (71%), followed by shrublands (17%), together comprising nearly 90% of the area. Greening trends are evident in 16% of the study area, concentrated primarily in the Northern Great Plains (NGP) grasslands (90% of the greening trend). Browning trends are minimal (1%).

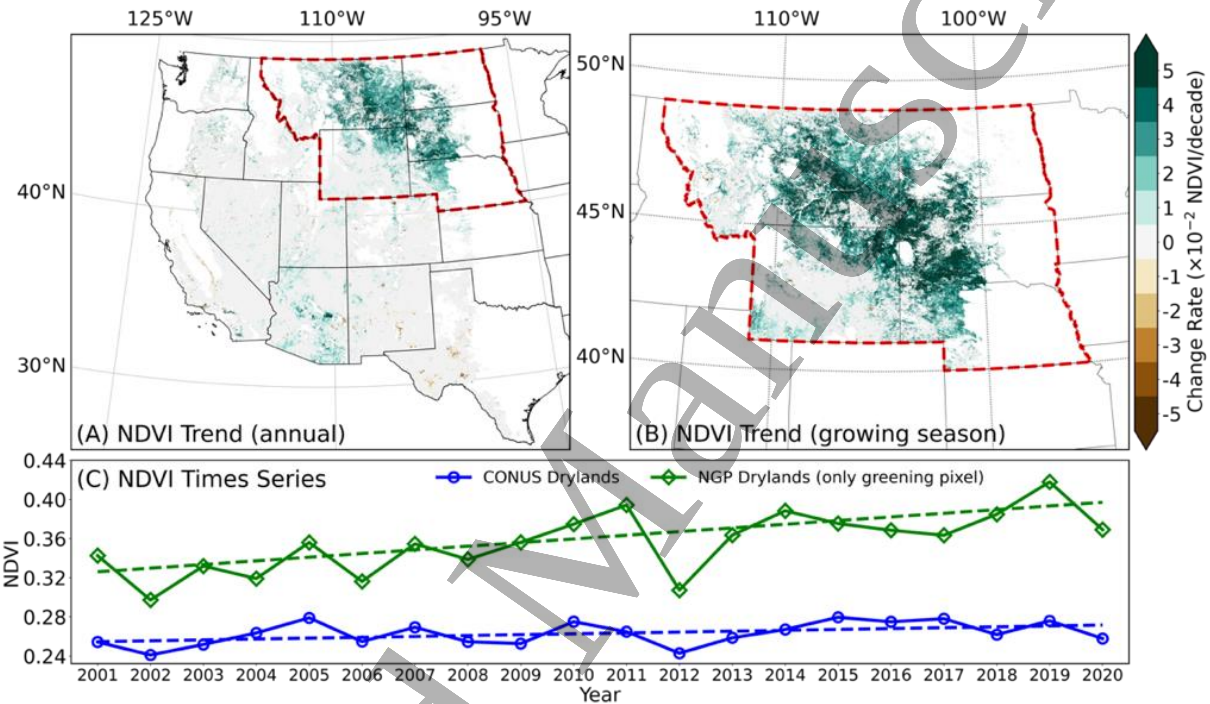

Figure 2. Results of NDVI trend analysis from 2001 to 2020. (A) Annual mean NDVI trend in CONUS drylands; (B) Growing season mean NDVI in the northern Great Plains (NGP) region; (C) Zonal-average NDVI time series for two regions of interest. The blue line represents the annual mean NDVI averaged over all pixels in CONUS drylands. The green line represents the growing season mean NDVI averaged over only greening pixels (P-value<0.1) in NGP drylands. The dashed lines are fitted regression lines according to MK test. The green line shows significant increasing trend (P-value < 0.1). The blue line doesn't show any significant trend.

Climate variables exhibit differed trends in the CONUS drylands (Figure 3). Among all three climate factors, precipitation is most strongly correlated with greening trends in CONUS drylands, especially in the NGP region. While some spatial inconsistencies exist due to differing data resolutions, the association between increased precipitation and vegetation greening is clear. Temperature shows less influence, and shortwave radiation exhibits a minor negative correlation with greening. Outside the NGP, precipitation trends are less significant, while temperature variations are observed in southern California, Arizona, New Mexico, and Texas. To understand the drivers of the significant greening trend in the Northern Great Plains (NGP), the MLR model is applied to greening pixels only. Analysis revealed weak but negligible correlation between climate variables, validating the variable independence assumption. The model effectively reproduced observed NDVI patterns (R-squared = 0.685) (Figure S3). Table 1 shows the values of coefficients from the attribution analysis. Precipitation is the dominant driver, with a significantly larger coefficient (0.8001) compared to temperature and radiation whose coefficients are close to zero (0.0169 for T, -0.0455 for R_{sw}), indicating minimal influence on the observed NDVI interannual variability. This highlights the importance of precipitation in driving vegetation greening in the NGP. The comparison of the interannual variability of NDVI and precipitation is provided in Figure S6.

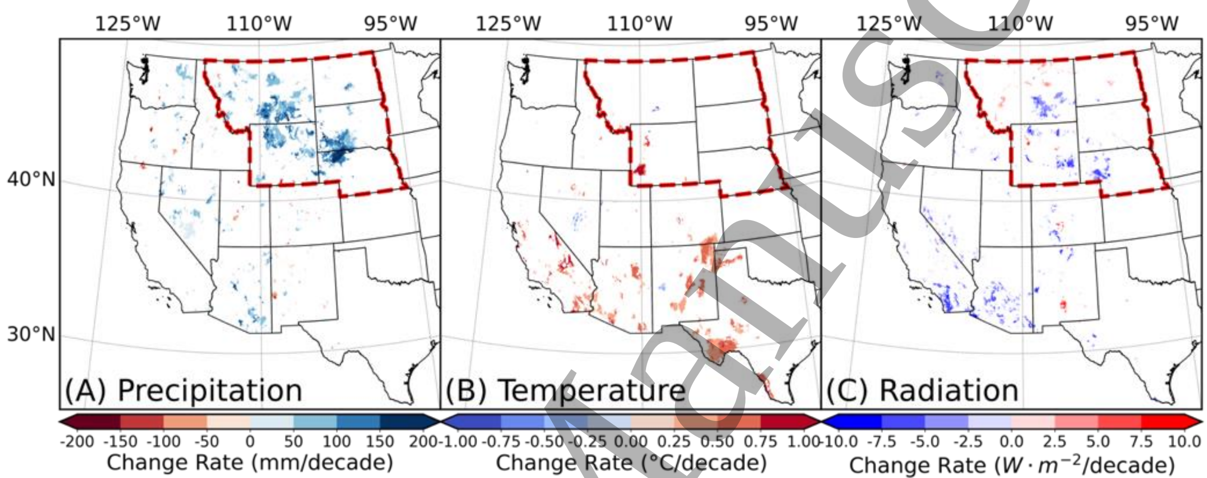

Figure 3. Trends of climate variables from 2001 to 2020. (A) Annual total precipitation; (B) Daily maximum temperature; (C) Shortwave radiation flux density.

Table 1. Results of the empirical linear attribution model

Coefficient	Value	P-value
α	<0.01	1
β_1	0.8001	0.037
β_2	0.0169	0.939
β_3	-0.0455	0.877

Note: α is the intercept term in the MLR model. Its close-to-zero value indicates the selected climate variables explain the most variability in NDVI anomalies. β_1, β_2 and β_3 are coefficients corresponding to anomalies of precipitation, temperature and shortwave radiation.

EOF analysis was conducted to further investigate the relationship between precipitation and NDVI in the NGP region, following the attribution model results. Figure 4 shows the EOF analysis. The first two EOF modes of both precipitation and NDVI capture the majority of the variance (72.7% and 69.8%, respectively), exhibiting similar spatial patterns and a high correlation (ρ=0.849) between their principal components (PCs). This confirms that interannual variability in seasonal NDVI is primarily driven by local precipitation, with no lagged effects. The first EOF mode for each variable also aligns with the spatial patterns observed in the trend analysis. The second EOF modes, while still highly correlated (ρ=0.809), reveal a latitudinal gradient in both precipitation and NDVI, suggesting the influence of other latitude-dependent climate factors on plant growth. However, the direct driver remains precipitation. From the third mode onwards, spatial correlations decrease significantly. The third EOF modes for precipitation and NDVI present similar regional clusters. This might indicates a weak topographic link between precipitation and NDVI variability at finer spatial scales.

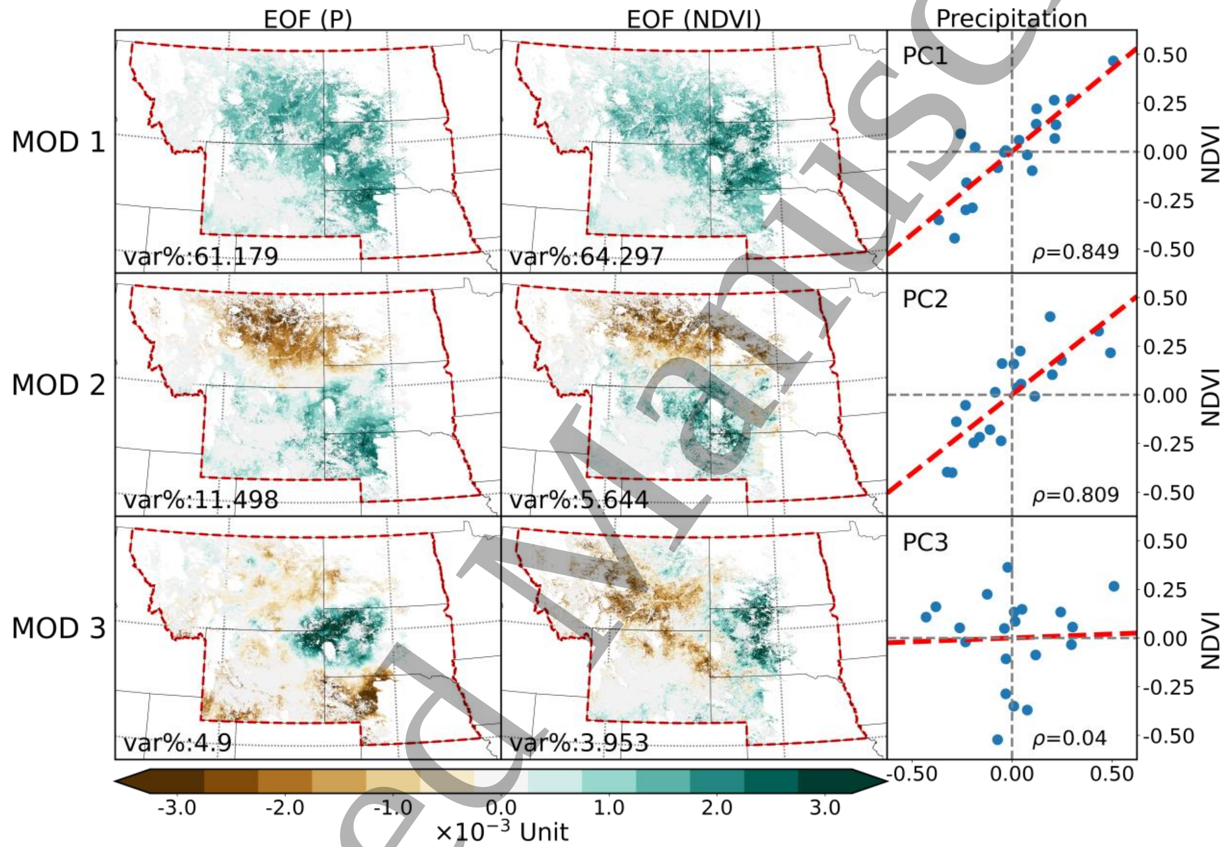

Figure 4. EOF analysis of seasonal precipitation and NDVI anomalies from 2001 to 2020. Only the results of the first three leading modes (EOF) and corresponding principal components (PC) for each variable are presented. The first two columns present the EOFs, and the third column presents the comparison of corresponding PCs.

Based on the combination of historical precipitation records and earth observations (EOs), precipitation in CONUS drylands is surely experiencing spatial shifting. Precipitation has become more unevenly distributed over the two-decade study period. Water availability in northern states, especially the NGP region, are progressively improved as the result of increase in precipitation, which theoretically increases the capacity of corresponding area to sustain denser and higher-level vegetation communities. In contrast, water scarcity for vegetation growth is expected to intensify in the southern states, including southern California, Arizona, New Mexico, and western Texas, mainly due to the widely observed increase in air temperature (Wahl et al., 2022; Zhuang et al., 2024). The local potential evapotranspiration becomes even higher because of the elevated vapor-pressure deficit (VPD) (Swain et al., 2025), which strengthens the water constraint on local plant growth.

Rain use efficiency patterns and CO_2 fertilization effect

Analysis reveals a significant linear relationship between precipitation and NDVI in our study regions over the two-decade period, evident from both annual (Appendix S4&S5) and climatological perspectives (Figure 5A&B). Strong correlations (exceeding 0.6) between climatological NDVI and precipitation suggest a stable long-term mean RUE, around which yearly values fluctuate. The wide shading areas (one standard deviation interval) in Figure 5C highlight substantial spatial variation in RUE, likely due to varying species composition and local environmental factors. Despite this variability, MK tests detect no significant RUE trends from 2001 to 2020 at the aggregated spatial scale (Figure 5C). Per-pixel trend analysis of RUE reveals greater spatial variation. While most pixels show no trend (Figure 6A), a significant number in the NGP region exhibit increasing annual mean RUE, largely coinciding with areas of increasing precipitation and NDVI. Although spatial discrepancies exist, annual and seasonal RUE trends in this region show broad similarity (Figure 6A&B). Notably, clusters of increasing seasonal RUE are concentrated further downstream along the Missouri River, compared to annual RUE. Outside the NGP region, increasing RUE is sparsely distributed, primarily along the 40°N latitude. Further south, declining RUE becomes more prevalent, particularly in southern California bordering Arizona, New Mexico, and Texas. This pattern of decline spatially overlay the increasing temperature trends in Figure 3B.

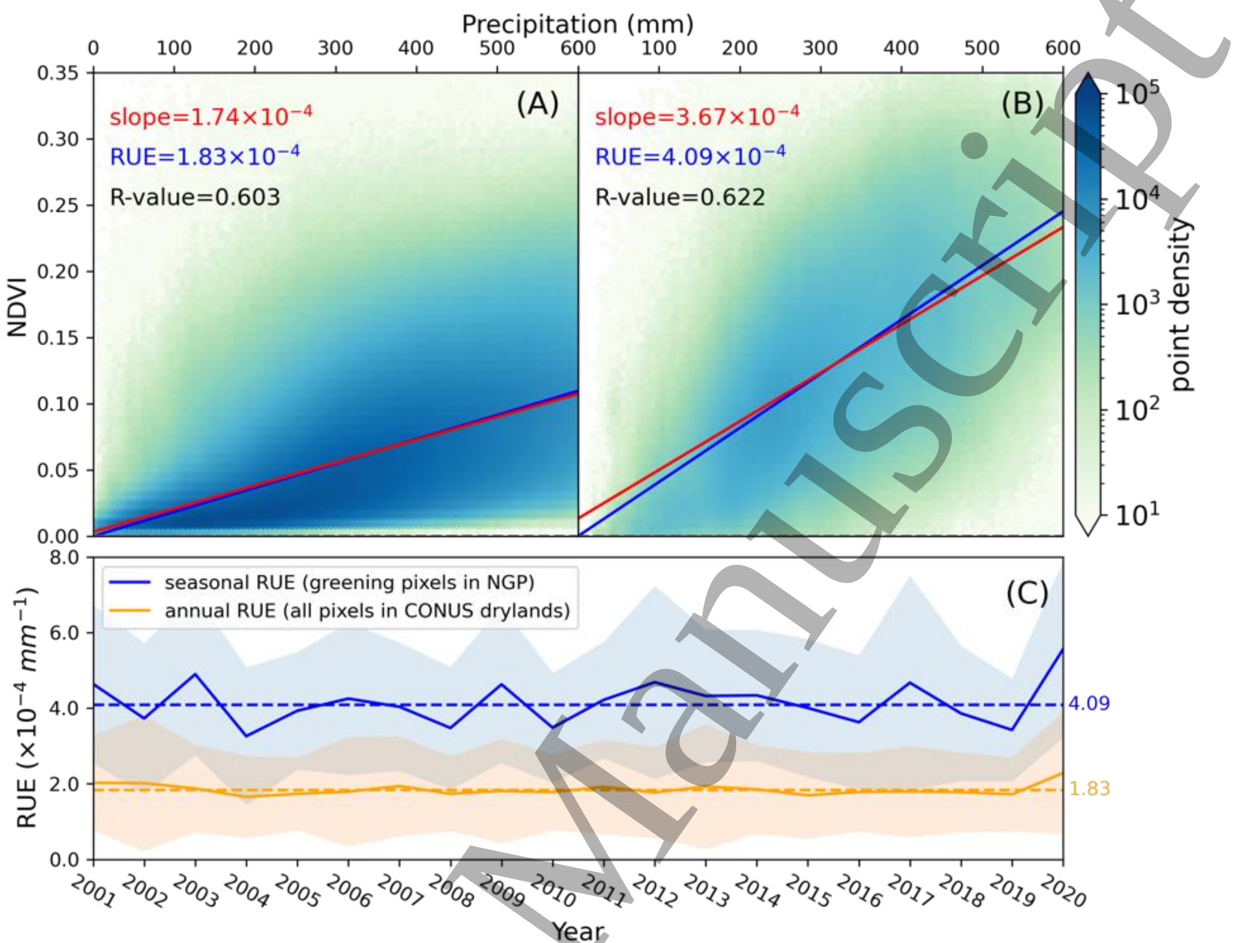

Figure 5. Rain use efficiency in the CONUS drylands and NGP region. (A) Scatter plot of climatology annual mean NDVI against annual total precipitation (ATP) in the CONUS drylands; (B) scatter plot of climatology growing season mean NDVI against growing season total precipitation for greening pixels only in the NGP region; (C) time series comparison of yearly annual mean RUE in CONUS drylands (orange line) and seasonal mean RUE in the NGP region (blue line, greening pixels only). The shading represents one standard deviation interval for each line. No trend is detected for both RUE time series by MK test (α=0.1).

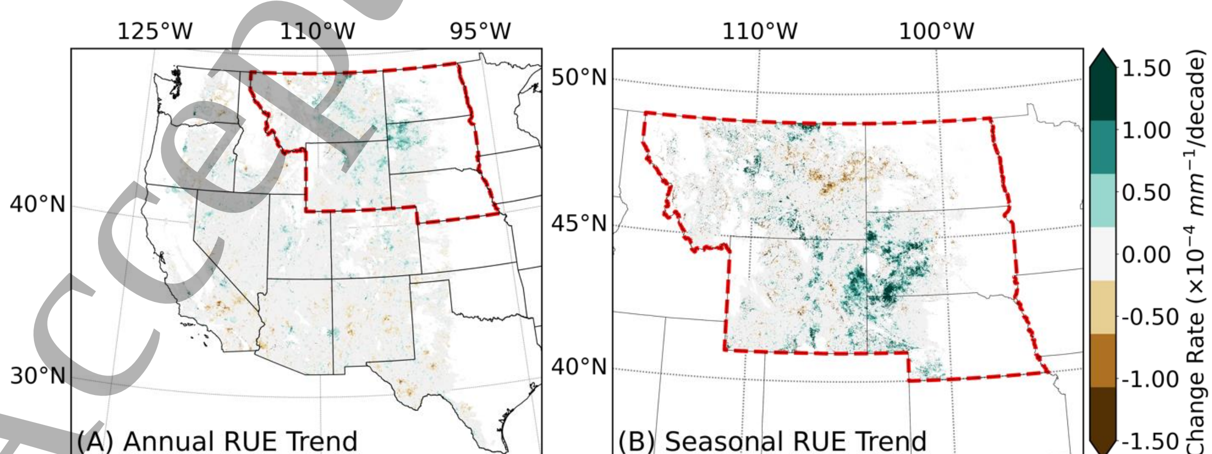

Figure 6. Per-pixel rain use efficiency trend analysis results. (A) Trend of annual mean RUE in the CONUS drylands; (B) Trend of seasonal mean RUE in the NGP region.

While a negative relationship between precipitation and RUE is often observed due to reduced water limitation (Huxman et al., 2004; Chen et al., 2020), the NGP region exhibits a contrasting pattern of increasing RUE alongside increasing precipitation. This suggests factors beyond simple water availability are at play. In drylands, high potential evapotranspiration and sparse vegetation can limit the translation of increased precipitation into significant improved plant growth (and RUE) (Zhu et al., 2022). A growing body of research has revealed the large-scale CO2 fertilization effect (CFE) in drylands (Rifai et al., 2022; Verbruggen et al., 2024; Uddin et al., 2018). It has been commonly accepted that CFE increases water use efficiency (WUE) through reducing stomatal conductance (Haverd et al., 2020). This phenomenon is expected to be more prominent in water limited areas, such as drylands, as local vegetation tends to save water while maintaining the level of photosynthesis. The observed RUE increase in the NGP region (Figure 6A&B) also points towards the CO_2 fertilization effect as a key driver (Zhang et al., 2022; Gonsamo et al., 2021). The potential CO2 fertilization effect in cool grasslands is echoing findings in Winkler et al., 2021. However, in contrast to expected large-scale decrease in RUE across CONUS drylands due to CFE, Figure 6A&B show that significant decreases in RUE are limited to areas with concurrent increases in precipitation (Figure 8C and Figure 9A). This highlights the complex interplay between water availability and CO_2 fertilization in driving vegetation dynamics in response to climate change in drylands.

If specifically considering the role of plant transpiration in RUE calculation, Eq. 2 can be re-rewritten as follow,

$$\mathrm{RUE} = \frac{\overline{\mathrm{NDVI}}}{\sum \mathrm{P}} = \frac{\overline{\mathrm{NDVI}}}{\sum \mathrm{E_T}} \cdot \frac{\sum \mathrm{E_T}}{\sum \mathrm{P}} \tag{6}$$

The increase in atmospheric CO_2 concentration affects plant growth in two major ways, reducing stomata conductance ($\frac{\sum E_T}{\sum P}$) by shortening the duration of stomata opening and stimulating vegetation cover ($\frac{\overline{NDVI}}{\sum E_T}$). Zhang et al., 2022 concluded that the increase in sensitivity of dryland vegetation greenness to precipitation is mainly because the stimulation effect overrides the decline in $\frac{\partial E_T}{\partial P}$ in those ecosystems. In our study region, except the NGP region, the simulation effect is limited as indicated by the relatively unchanged NDVI. The water use efficiency ($\frac{\overline{NDVI}}{\sum E_T}$) of local plants may have increased so that it compensates for the decrease in stomata conductance, but not to the point where the RUE also shows significant changes.

The above explanation assumes that vegetation in drylands aims to maximize water use efficiency (WUE) and that CFE suppresses stomatal conductance, consistent with the traditional optimality theory of plants (Cowan & Farquhar, 1977). However, Wolf et al. (2016) propose that under conditions of intense water competition—driven by high evaporative demand and competition from neighboring plants—a more evolutionarily advantageous strategy for plants may be to prioritize maximizing growth rate by increasing stomatal conductance, even at the cost of reduced WUE. The absence of a large-scale increase in resource use efficiency (RUE) and the spatially correlated increase in RUE with precipitation in the NGP region (Figure 6A&B) may reflect this theory at the ecosystem scale. This suggests that alleviating water limitations could be a prerequisite for dryland ecosystems to fully benefit from elevated CO_2 concentrations. To reach a decisive conclusion requires a thorough quantitative analysis of the long-term stomatal behavior of local vegetation, accounting for the plant hydraulic stress imposed by scare soil moisture in drylands.

The similarity in the spatial distributions of the decreasing RUE and increasing temperature patterns observed in the southern states implies their physiological connections. The influence of temperature on RUE is complicated, as optimum temperature ranges exist for all biomes, in which vegetation balances it carbonate production and water loss through stomata. Drylands in southern states are characterized by excessive temperature and dry environments. Increasing temperature in water limited region strengthens the need for plant to preserve water through further reducing the stomata conductance. As a result, the intercellular CO_2 concentration won’t always be as high as atmospheric CO_2 concentration, which reduces $\frac{\overline{NDVI}}{\sum E_T}$. The combined effect of intensified reduction of $\frac{\sum E_T}{\sum P}$ and further limited $\frac{\overline{NDVI}}{\sum E_T}$ entails the observed decrease in RUE in southern states.

Modeling and projections

The proposed model aims to quantify the interannual variability of NDVI in CONUS drylands using precipitation as the sole independent variable. Model performance is evaluated across both temporal and spatial domains. We first use the model to reproduce the time series of observed spatial-average NDVI for two regions: the NGP (using growing season mean NDVI) and the entire CONUS drylands (using annual mean NDVI). As presented in Table 2, there are 61888211 and 16742453 valid pixels in total used for parameter estimation in two different cases. Their respective R-squared values are 0.721 and 0.859, indicating good model fit. The estimated climatological RUE (β_0) (Table 2) closely match values derived directly from the data (Figure 5C). Figure 7 further demonstrates strong agreement between observed and modeled spatial-average NDVI times series over time. The model effectively reproduces the spatial-average NDVI time series in both regions, exhibiting high R2 values (0.825 for NGP and 0.9 for CONUS), low RMSE (0.014 and 0.004), and low NRMSE (0.125 and 0.112). These results confirm the model's ability to capture the temporal dynamics of NDVI. To assess the model's ability to capture spatial heterogeneity, we applied it at the pixel level across the entire study region (Figure 8). R-squared values exceed 0.5 for most pixels (Figure 8A). After excluding pixels with insufficient data or invalid parameters, the relative error between modeled and observed climatological annual mean NDVI remains below 10% for most areas, with some overestimation (around 10%) observed in the NGP region (Figure 8B). Overall, the proposed model demonstrates robust performance in capturing the interannual variability of NDVI in CONUS drylands, both temporally and spatially, underscoring the critical role of water availability in driving vegetation dynamics.

Table 2. Modeling results in two study regions

Results	Region	
	NGP	CONUS
# of pixels	16742453	61888211
R^2	0.721	0.859
Intercept	-0.009	-0.011
α	0.966	1.037
k	-2.620×10^{-7}	-7.220×10^{-8}
β_0	4.721×10^{-4}	1.970×10^{-4}

Note: α, k, and β_0 in the above table are estimated parameters, representing the persistence rate of greenness, the sensitivity of RUE to precipitation anomaly, and climatology RUE

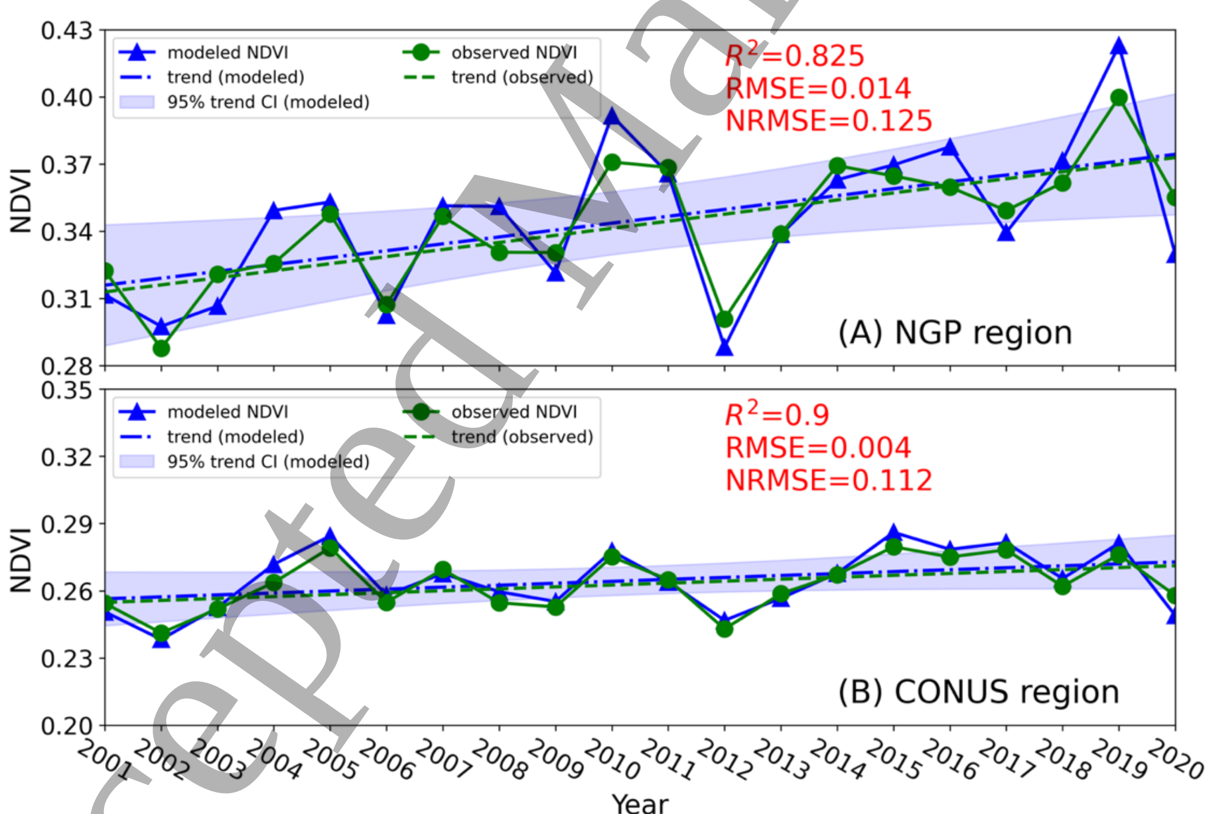

Figure 7. Comparison of observed and modeled NDVI interannual variability in (A) NGP and (B) CONUS dryland regions. The trend lines for observed and modeled NDVI, as estimated through linear regression in both panels, exhibit a high degree of overlap. Significant increasing trends are detected in both observed and modeled in (A) by MK test. No significant trends are detected in (B) by MK test.

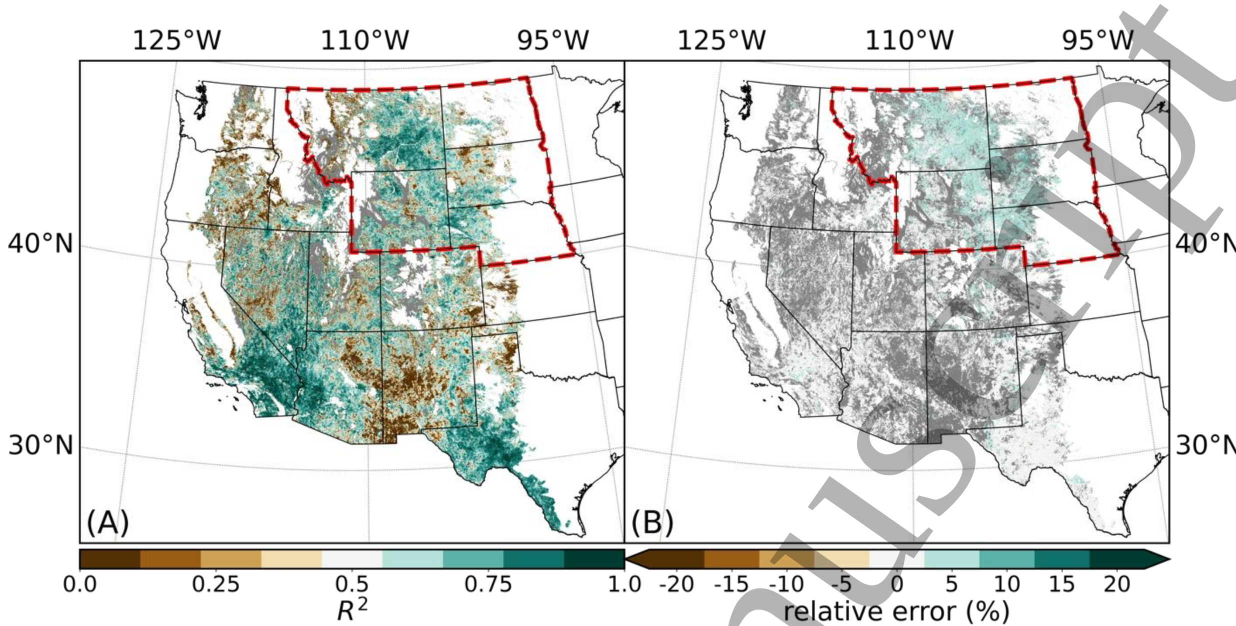

Figure 8. Per-pixel modeling results in the CONUS drylands. (A) presents the coefficient of determination (R^2) at each pixel; (B) presents the relative error between observed and modeled climatology annual mean NDVI (2001~2020) in percentage. Shaded area (gray) in (A) represents masked pixels which have less than 15 valid NDVI observations out of 20 years. Shaded area (gray) in (B) represents masked pixels that combine the shaded area in (A) and pixels with R^2 lower than 0.5 or negative estimated β_0 (RUE).

The model's success in reproducing observed NDVI patterns validates its utility for understanding and predicting vegetation responses to precipitation variability, particularly in light of future CMIP6 projections that indicate a potential reversal of recent greening trends. These projections, based on averaging predictions from six different models (GFDL-ESM4 MIROC6, MPI-ESM1-2-HR, EC_Earth3-Veg, UKESM1-0-LL, and CMCC-ESM2) under the SSP370 scenario, show a widespread decrease in climatological annual total precipitation (ATP) of approximately 20% in the NGP region (Figure 9A), with corresponding declines in NDVI of up to 10% (Figure 9B). This potential browning trend, contrasting with the observed greening, could have significant implications for ecosystem services and carbon sequestration in the NGP and Midwest. While some southern states may experience localized vegetation increases due to increased precipitation, the limited extent of these areas underscores the overall vulnerability of CONUS drylands to future climate change.

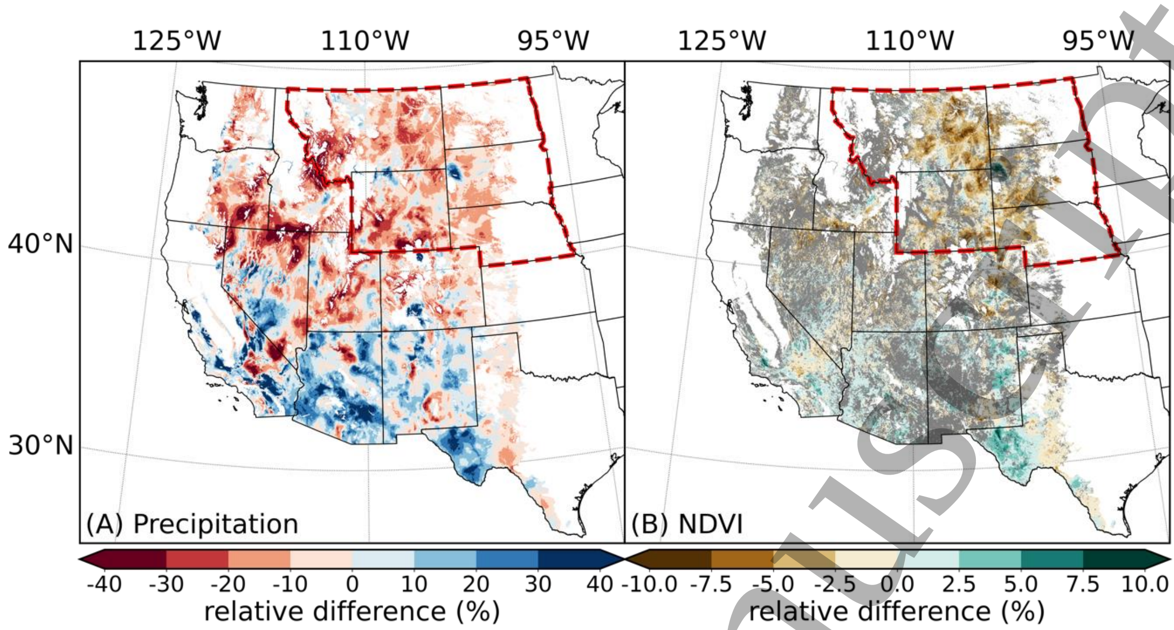

Figure 9. Relative differences between (A) climatology annual total precipitation of the study period (2001~2020) and CMIP6 climatology projection (2021~2040), and (B) climatology NDVI of the study period and projected NDVI estimated by per-pixel model, using CMIP6 climatology precipitation projection (2021~2040) as input. Shaded area (gray) in (B) represents masked pixels in Figure 8B. CMIP6 climatology precipitation projection is taken as the average of precipitation simulations of different GCMs under SSP370 scenario.

It is important to acknowledge that these projections rely on simplified assumptions and do not account for potential shifts in vegetation communities or factors like CO_2 fertilization. While demonstrating strong predictive power, the model's reliance on precipitation as the sole predictor also highlights a potential limitation. Future research could incorporate additional variables, such as temperature and soil moisture, to enhance its accuracy and applicability.

Conclusion

This study utilizes 20-year MODIS NDVI data and high-resolution meteorological data (1-km) to analyze long-term vegetation changes in conterminous United States (CONUS) drylands and their responses to climate variability. We find substantial greening trends across the Northern Great Plains (NGP) from 2001 to 2020, primarily driven by increased precipitation. Temperature and shortwave radiation exert secondary influences on NDVI by modulating local precipitation patterns. While rising CO_2 appears to enhance RUE in NGP region where increase trends of precipitation is also present, decreases in RUE across southern states correlate with rising temperatures, highlighting the complex interplay of climate factors on vegetation. Although CO_2 fertilization effect (CFE) is expected to promote vegetation growth in drylands by enhancing water-use efficiency, the extent of this effect depends on local environmental conditions, particularly water availability, which is in contrast with large-scale CFE in drylands concluded in studies using coarser resolution products. These discrepancies also suggest the important role of stomatal behavior in understanding the adaptation of vegetation in drylands to changing climate. Our efficiency-based model effectively quantifies NDVI variability, emphasizing the critical role of water availability in dryland ecosystems. However, CMIP6-based projections using this model suggest potential future browning in the NGP region and areas near 42°N latitude, contrasting with recent greening trends. This underscores the vulnerability of these ecosystems to future climate change, although adaptive capacity and human interventions may modulate these outcomes. Our findings highlight the need for adaptive management strategies to mitigate potential negative impacts on dryland vegetation and emphasize the importance of incorporating additional factors into future models for enhanced accuracy.

Competing Interests

The authors declare no conflict of interests.

Acknowledgements

The authors acknowledge funding from NASA Earth Science Division to Boston University under the MODIS (9500312733) and VIIRS (9500312663) Programs.

Reference

1. Ahlström, A., Raupach, M. R., Schurgers, G., Smith, B., Arneth, A., Jung, M., Reichstein, M., Canadell, J. G., Friedlingstein, P., Jain, A. K., Kato, E., Poulter, B., Sitch, S., Stocker, B. D., Viovy, N., Wang, Y. P., Wiltshire, A., Zaehle, S., & Zeng, N. (2015). The dominant role of semi-arid ecosystems in the trend and variability of the land CO2 sink. *Science*, *348*(6237), 895–899. https://doi.org/10.1126/science.aaa1668
2. Berdugo, M., Delgado-Baquerizo, M., Soliveres, S., Hernández-Clemente, R., Zhao, Y., Gaitán, J. J., Gross, N., Saiz, H., Maire, V., Lehmann, A., Rillig, M. C., Solé, R. V., & Maestre, F. T. (2020). Global ecosystem thresholds driven by aridity. *Science*, *367*(6479), 787–790. https://doi.org/10.1126/science.aay5958
3. Berg, A., & McColl, K. A. (2021). No projected global drylands expansion under greenhouse warming. *Nature Climate Change*, *11*(4), 331–337. https://doi.org/10.1038/s41558-021-01007-8
4. Bradford, J. B., Schlaepfer, D. R., Lauenroth, W. K., & Palmquist, K. A. (2020). Robust ecological drought projections for drylands in the 21st century. *Global Change Biology*, *26*(7), 3906–3919. https://doi.org/10.1111/gcb.15075
5. Burrell, A. L., Evans, J. P., & De Kauwe, M. G. (2020). Anthropogenic climate change has driven over 5 million km2 of drylands towards desertification. *Nature Communications*, *11*(1), 3853. https://doi.org/10.1038/s41467-020-17710-7
6. Canty, T., Mascioli, N. R., Smarte, M. D., & Salawitch, R. J. (2013). An empirical model of global climate – Part 1: A critical evaluation of volcanic cooling. *Atmospheric Chemistry and Physics*, *13*(8), 3997–4031. https://doi.org/10.5194/acp-13-3997-2013
7. Chang, J., Tian, J., Zhang, Z., Chen, X., Chen, Y., Chen, S., & Duan, Z. (2018). Changes of Grassland Rain Use Efficiency and NDVI in Northwestern China from 1982 to 2013 and Its Response to Climate Change. *Water*, *10*(11), 1689. https://doi.org/10.3390/w10111689
8. Chen, C., Park, T., Wang, X., Piao, S., Xu, B., Chaturvedi, R. K., Fuchs, R., Brovkin, V., Ciais, P., Fensholt, R., Tømmervik, H., Bala, G., Zhu, Z., Nemani, R. R., & Myneni, R. B. (2019). China and India lead in greening of the world through land-use management. *Nature Sustainability*, *2*(2), 122–129. https://doi.org/10.1038/s41893-019-0220-7
9. Chen, J., Jönsson, Per., Tamura, M., Gu, Z., Matsushita, B., & Eklundh, L. (2004). A simple method for reconstructing a high-quality NDVI time-series data set based on the Savitzky–Golay filter. *Remote Sensing of Environment*, *91*(3), 332–344. https://doi.org/10.1016/j.rse.2004.03.014
10. Chen, Z., Wang, W., Yu, Z., Xia, J., & Schwartz, F. W. (2020). The collapse points of increasing trend of vegetation rain-use efficiency under droughts. *Environmental Research Letters*, *15*(10), 104072. https://doi.org/10.1088/1748-9326/abb332
11. Cowan, I. R., & Farquhar, G. D. (1977). Stomatal function in relation to leaf metabolism and environment. *Symposia of the Society for Experimental Biology*, *31*, 471–505.
12. Dardel, C., Kergoat, L., Hiernaux, P., Grippa, M., Mougin, E., Ciais, P., & Nguyen, C.-C. (2014). Rain-Use-Efficiency: What it Tells us about the Conflicting Sahel Greening and Sahelian Paradox. *Remote Sensing*, *6*(4), 3446–3474. https://doi.org/10.3390/rs6043446
13. Dawson, A. (2016). *eofs: A Library for EOF Analysis of Meteorological, Oceanographic, and Climate Data*. *4*(1), e14. https://doi.org/10.5334/jors.122

14. de Jong, R., de Bruin, S., de Wit, A., Schaepman, M. E., & Dent, D. L. (2011). Analysis of monotonic greening and browning trends from global NDVI time-series. *Remote Sensing of Environment*, *115*(2), 692–702. https://doi.org/10.1016/j.rse.2010.10.011
15. Didan, K. (2021). *MODIS/Terra Vegetation Indices 16-Day L3 Global 250m SIN Grid V061* [Dataset]. NASA EOSDIS Land Processes Distributed Active Archive Center. https://doi.org/10.5067/MODIS/MOD13Q1.061
16. Eyring, V., Bony, S., Meehl, G. A., Senior, C. A., Stevens, B., Stouffer, R. J., & Taylor, K. E. (2016). Overview of the Coupled Model Intercomparison Project Phase 6 (CMIP6) experimental design and organization. *Geoscientific Model Development*, *9*(5), 1937–1958. https://doi.org/10.5194/gmd-9-1937-2016
17. Feng, S., & Fu, Q. (2013). Expansion of global drylands under a warming climate. *Atmospheric Chemistry and Physics*, *13*(19), 10081–10094. https://doi.org/10.5194/acp-13-10081-2013
18. Fensholt, R., Langanke, T., Rasmussen, K., Reenberg, A., Prince, S. D., Tucker, C., Scholes, R. J., Le, Q. B., Bondeau, A., Eastman, R., Epstein, H., Gaughan, A. E., Hellden, U., Mbow, C., Olsson, L., Paruelo, J., Schweitzer, C., Seaquist, J., & Wessels, K. (2012). Greenness in semi-arid areas across the globe 1981–2007—An Earth Observing Satellite based analysis of trends and drivers. *Remote Sensing of Environment*, *121*, 144–158. https://doi.org/10.1016/j.rse.2012.01.017
19. Fensholt, R., Rasmussen, K., Kaspersen, P., Huber, S., Horion, S., & Swinnen, E. (2013). Assessing Land Degradation/Recovery in the African Sahel from Long-Term Earth Observation Based Primary Productivity and Precipitation Relationships. *Remote Sensing*, *5*(2), 664–686. https://doi.org/10.3390/rs5020664
20. Fick, S. E., & Hijmans, R. J. (2017). WorldClim 2: New 1-km spatial resolution climate surfaces for global land areas. *International Journal of Climatology*, *37*(12), 4302–4315. https://doi.org/10.1002/joc.5086
21. Friedl, M., & Sulla-Menashe, D. (2022). *MODIS/Terra+Aqua Land Cover Type Yearly L3 Global 500m SIN Grid V061* [Dataset]. NASA EOSDIS Land Processes Distributed Active Archive Center. https://doi.org/10.5067/MODIS/MCD12Q1.061
22. Gonsamo, A., Ciais, P., Miralles, D. G., Sitch, S., Dorigo, W., Lombardozzi, D., Friedlingstein, P., Nabel, J. E. M. S., Goll, D. S., O'Sullivan, M., Arneth, A., Anthoni, P., Jain, A. K., Wiltshire, A., Peylin, P., & Cescatti, A. (2021). Greening drylands despite warming consistent with carbon dioxide fertilization effect. *Global Change Biology*, *27*(14), 3336–3349. https://doi.org/10.1111/gcb.15658
23. Hänke, H., Börjeson, L., Hylander, K., & Enfors-Kautsky, E. (2016). Drought tolerant species dominate as rainfall and tree cover returns in the West African Sahel. *Land Use Policy*, *59*, 111–120. https://doi.org/10.1016/j.landusepol.2016.08.023
24. Haverd, V., Smith, B., Canadell, J. G., Cuntz, M., Mikaloff-Fletcher, S., Farquhar, G., Woodgate, W., Briggs, P. R., & Trudinger, C. M. (2020). Higher than expected CO_2 fertilization inferred from leaf to global observations. *Global Change Biology*, *26*(4), 2390–2402. https://doi.org/10.1111/gcb.14950
25. He, B., Wang, S., Guo, L., & Wu, X. (2019). Aridity change and its correlation with greening over drylands. *Agricultural and Forest Meteorology*, *278*, 107663. https://doi.org/10.1016/j.agrformet.2019.107663
26. Holm, A. M., Cridland, S. W., & Roderick, M. L. (2003). The use of time-integrated NOAA NDVI data and rainfall to assess landscape degradation in the arid shrubland of Western

Australia. *Remote Sensing of Environment*, *85*(2), 145–158. https://doi.org/10.1016/S0034-4257(02)00199-2
27. Hussain, M. M., & Mahmud, I. (2019). pyMannKendall: A python package for non parametric Mann Kendall family of trend tests. *Journal of Open Source Software*, *4*(39), 1556. https://doi.org/10.21105/joss.01556
28. Huxman, T. E., Smith, M. D., Fay, P. A., Knapp, A. K., Shaw, M. R., Loik, M. E., Smith, S. D., Tissue, D. T., Zak, J. C., Weltzin, J. F., Pockman, W. T., Sala, O. E., Haddad, B. M., Harte, J., Koch, G. W., Schwinning, S., Small, E. E., & Williams, D. G. (2004). Convergence across biomes to a common rain-use efficiency. *Nature*, *429*(6992), 651–654. https://doi.org/10.1038/nature02561
29. Ji, L., & Brown, J. F. (2022). *Temporal Greenness Trends in Stable Natural Land Cover and Relationships with Climatic Variability across the Conterminous United States*. https://doi.org/10.1175/EI-D-21-0018.1
30. Korell, L., Auge, H., Chase, J. M., Harpole, W. S., & Knight, T. M. (2021). Responses of plant diversity to precipitation change are strongest at local spatial scales and in drylands. *Nature Communications*, *12*(1), 2489. https://doi.org/10.1038/s41467-021-22766-0
31. Körner, C., Möhl, P., & Hiltbrunner, E. (2023). Four ways to define the growing season. *Ecology Letters*, *26*(8), 1277–1292. https://doi.org/10.1111/ele.14260
32. Le Houérou, H. N. (1984). Rain use efficiency: A unifying concept in arid-land ecology. *Journal of Arid Environments*, *7*(3), 213–247. https://doi.org/10.1016/S0140-1963(18)31362-4
33. Lean, J. L., & Rind, D. H. (2008). How natural and anthropogenic influences alter global and regional surface temperatures: 1889 to 2006. *Geophysical Research Letters*, *35*(18). https://doi.org/10.1029/2008GL034864
34. Lehner, F., Coats, S., Stocker, T. F., Pendergrass, A. G., Sanderson, B. M., Raible, C. C., & Smerdon, J. E. (2017). Projected drought risk in 1.5°C and 2°C warmer climates. *Geophysical Research Letters*, *44*(14), 7419–7428. https://doi.org/10.1002/2017GL074117
35. Li, Z., Wang, S., Li, C., Ye, C., Gao, D., & Chen, P. (2022). The trend shift caused by ecological restoration accelerates the vegetation greening of China's drylands since the 1980s. *Environmental Research Letters*, *17*(4), 044062. https://doi.org/10.1088/1748-9326/ac6002
36. Lian, X., Piao, S., Chen, A., Huntingford, C., Fu, B., Li, L. Z. X., Huang, J., Sheffield, J., Berg, A. M., Keenan, T. F., McVicar, T. R., Wada, Y., Wang, X., Wang, T., Yang, Y., & Roderick, M. L. (2021). Multifaceted characteristics of dryland aridity changes in a warming world. *Nature Reviews Earth & Environment*, *2*(4), 232–250. https://doi.org/10.1038/s43017-021-00144-0
37. Müller, L. M., & Bahn, M. (2022). Drought legacies and ecosystem responses to subsequent drought. *Global Change Biology*, *28*(17), 5086–5103. https://doi.org/10.1111/gcb.16270
38. Myneni, R. B., & Williams, D. L. (1994). On the relationship between FAPAR and NDVI. *Remote Sensing of Environment*, *49*(3), 200–211. https://doi.org/10.1016/0034-4257(94)90016-7
39. Nemani, R. R., Keeling, C. D., Hashimoto, H., Jolly, W. M., Piper, S. C., Tucker, C. J., Myneni, R. B., & Running, S. W. (2003). Climate-Driven Increases in Global Terrestrial Net Primary Production from 1982 to 1999. *Science*, *300*(5625), 1560–1563. https://doi.org/10.1126/science.1082750
40. O'Neill, B. C., Tebaldi, C., van Vuuren, D. P., Eyring, V., Friedlingstein, P., Hurtt, G., Knutti, R., Kriegler, E., Lamarque, J.-F., Lowe, J., Meehl, G. A., Moss, R., Riahi, K., & Sanderson, B.

M. (2016). The Scenario Model Intercomparison Project (ScenarioMIP) for CMIP6. *Geoscientific Model Development*, *9*(9), 3461–3482. https://doi.org/10.5194/gmd-9-3461-2016

41. Paruelo, J. M., Lauenroth, W. K., Burke, I. C., & Sala, O. E. (1999). Grassland Precipitation-Use Efficiency Varies Across a Resource Gradient. *Ecosystems*, *2*(1), 64–68. https://doi.org/10.1007/s100219900058
42. PRINCE, S. D. (2007). Satellite remote sensing of primary production: Comparison of results for Sahelian grasslands 1981-1988. *International Journal of Remote Sensing*. https://doi.org/10.1080/01431169108929727
43. Rasmussen, M. S. (2010). Developing simple, operational, consistent NDVI-vegetation models by applying environmental and climatic information: Part I. Assessment of net primary production. *International Journal of Remote Sensing*. https://doi.org/10.1080/014311698216459
44. Rifai, S. W., De Kauwe, M. G., Ukkola, A. M., Cernusak, L. A., Meir, P., Medlyn, B. E., & Pitman, A. J. (2022). Thirty-eight years of CO_2 fertilization has outpaced growing aridity to drive greening of Australian woody ecosystems. *Biogeosciences*, *19*(2), 491–515. https://doi.org/10.5194/bg-19-491-2022
45. Roundy, P. E. (2015). On the Interpretation of EOF Analysis of ENSO, Atmospheric Kelvin Waves, and the MJO. *Journal of Climate*, *28*(3), 1148–1165. https://doi.org/10.1175/JCLI-D-14-00398.1
46. Stern, D. I., & Kaufmann, R. K. (2014). Anthropogenic and natural causes of climate change. *Climatic Change*, *122*(1), 257–269. https://doi.org/10.1007/s10584-013-1007-x
47. Swain, D. L., Prein, A. F., Abatzoglou, J. T., Albano, C. M., Brunner, M., Diffenbaugh, N. S., Singh, D., Skinner, C. B., & Touma, D. (2025). Hydroclimate volatility on a warming Earth. *Nature Reviews Earth & Environment*, *6*(1), 35–50. https://doi.org/10.1038/s43017-024-00624-z
48. Thornton, M. M., Shrestha, R., Wei, Y., Thornton, P. E., Kao, S.-C., & Wilson, B. E. (2022). *Daymet: Daily Surface Weather Data on a 1-km Grid for North America, Version 4 R1*. 0 MB. https://doi.org/10.3334/ORNLDAAC/2129
49. Thornton, P. E., Shrestha, R., Thornton, M., Kao, S.-C., Wei, Y., & Wilson, B. E. (2021). Gridded daily weather data for North America with comprehensive uncertainty quantification. *Scientific Data*, *8*(1), 190. https://doi.org/10.1038/s41597-021-00973-0
50. Tippett, M. K., & L'Heureux, M. L. (2020). Low-dimensional representations of Niño 3.4 evolution and the spring persistence barrier. *Npj Climate and Atmospheric Science*, *3*(1), 1–11. https://doi.org/10.1038/s41612-020-0128-y
51. Uddin, S., Löw, M., Parvin, S., Fitzgerald, G. J., Tausz-Posch, S., Armstrong, R., O'Leary, G., & Tausz, M. (2018). Elevated [CO2] mitigates the effect of surface drought by stimulating root growth to access sub-soil water. *PLOS ONE*, *13*(6), e0198928. https://doi.org/10.1371/journal.pone.0198928
52. Verbruggen, W., Schurgers, G., Meunier, F., Verbeeck, H., & Horion, S. (2024). Simulated Tree-Grass Competition in Drylands Is Modulated by CO_2 Fertilization. *Earth's Future*, *12*(1), e2023EF004096. https://doi.org/10.1029/2023EF004096
53. Verón, S. R., Oesterheld, M., & Paruelo, J. M. (2005). Production as a function of resource availability: Slopes and efficiencies are different. *Journal of Vegetation Science*, *16*(3), 351–354. https://doi.org/10.1111/j.1654-1103.2005.tb02373.x

54. Volkov, D. L., Schmid, C., Chomiak, L., Germineaud, C., Dong, S., & Goes, M. (2022). Interannual to decadal sea level variability in the subpolar North Atlantic: The role of propagating signals. *Ocean Science*, *18*(6), 1741–1762. https://doi.org/10.5194/os-18-1741-2022
55. Wahl, E. R., Zorita, E., Diaz, H. F., & Hoell, A. (2022). Southwestern United States drought of the 21st century presages drier conditions into the future. *Communications Earth & Environment*, *3*(1), 1–14. https://doi.org/10.1038/s43247-022-00532-4
56. Werb, B. E., & Rudnick, D. L. (2023). Remarkable Changes in the Dominant Modes of North Pacific Sea Surface Temperature. *Geophysical Research Letters*, *50*(4), e2022GL101078. https://doi.org/10.1029/2022GL101078
57. Wessels, K. J., Prince, S. D., Zambatis, N., MacFadyen, S., Frost, P. E., & Van Zyl, D. (2006). Relationship between herbaceous biomass and 1-km2 Advanced Very High Resolution Radiometer (AVHRR) NDVI in Kruger National Park, South Africa. *International Journal of Remote Sensing*, *27*(5), 951–973. https://doi.org/10.1080/01431160500169098
58. Winkler, A. J., Myneni, R. B., Hannart, A., Sitch, S., Haverd, V., Lombardozzi, D., Arora, V. K., Pongratz, J., Nabel, J. E. M. S., Goll, D. S., Kato, E., Tian, H., Arneth, A., Friedlingstein, P., Jain, A. K., Zaehle, S., & Brovkin, V. (2021). Slowdown of the greening trend in natural vegetation with further rise in atmospheric CO_2. *Biogeosciences*, *18*(17), 4985–5010. https://doi.org/10.5194/bg-18-4985-2021
59. Wolf, A., Anderegg, W. R. L., & Pacala, S. W. (2016). Optimal stomatal behavior with competition for water and risk of hydraulic impairment. *Proceedings of the National Academy of Sciences*, *113*(46). https://doi.org/10.1073/pnas.1615144113
60. Xue, J., Ge, Y., & Ren, H. (2017). Spatial upscaling of green aboveground biomass derived from MODIS-based NDVI in arid and semiarid grasslands. *Advances in Space Research*, *60*(9), 2001–2008. https://doi.org/10.1016/j.asr.2017.07.016
61. Yue, S., Pilon, P., Phinney, B., & Cavadias, G. (2002). The influence of autocorrelation on the ability to detect trend in hydrological series. *Hydrological Processes*, *16*(9), 1807–1829. https://doi.org/10.1002/hyp.1095
62. Zhang, J., Zhang, Y., Cong, N., Tian, L., Zhao, G., Zheng, Z., Gao, J., Zhu, Y., & Zhang, Y. (2023). Coarse spatial resolution remote sensing data with AVHRR and MODIS miss the greening area compared with the Landsat data in Chinese drylands. *Frontiers in Plant Science*, *14*. https://doi.org/10.3389/fpls.2023.1129665
63. Zhang, X., Du, X., & Zhu, Z. (2020). Effects of precipitation and temperature on precipitation use efficiency of alpine grassland in Northern Tibet, China. *Scientific Reports*, *10*(1), 20309. https://doi.org/10.1038/s41598-020-77208-6
64. Zhang, Y., Gentine, P., Luo, X., Lian, X., Liu, Y., Zhou, S., Michalak, A. M., Sun, W., Fisher, J. B., Piao, S., & Keenan, T. F. (2022). Increasing sensitivity of dryland vegetation greenness to precipitation due to rising atmospheric CO2. *Nature Communications*, *13*(1), 4875. https://doi.org/10.1038/s41467-022-32631-3
65. Zhang, Y., Wallace, J. M., & Battisti, D. S. (1997). ENSO-like Interdecadal Variability: 1900–93. *Journal of Climate*, *10*(5), 1004–1020. https://doi.org/10.1175/1520-0442(1997)010<1004:ELIV>2.0.CO;2
66. Zhu, X., Liu, H., Xu, C., Wu, L., Shi, L., & Liu, F. (2022). Soil coarsening alleviates precipitation constraint on vegetation growth in global drylands. *Environmental Research Letters*, *17*(11), 114008. https://doi.org/10.1088/1748-9326/ac953f

67. Zhuang, Y., Fu, R., Lisonbee, J., Sheffield, A. M., Parker, B. A., & Deheza, G. (2024). Anthropogenic warming has ushered in an era of temperature-dominated droughts in the western United States. *Science Advances*, *10*(45), eadn9389. https://doi.org/10.1126/sciadv.adn9389